Photochemical ozone budget during the BIBLE A and B campaigns

Malcolm Ko,[1,2] Wenjie Hu,[1,3] José M. Rodríguez,[4] Yutaka Kondo,[5] Makoto Koike,[6] Kazuyuki Kita,[5] Shuji Kawakami,[7] Donald Blake,[8] Shaw Liu,[9] and Toshihiro Ogawa[7]

Received 2 May 2001; revised 28 January 2002; accepted 20 March 2002; published 24 December 2002.

[1] Using the measured concentrations of NO, O_3, H_2O, CO, CH_4, and NMHCs along the flight tracks, a photochemical box model is used to calculate the concentrations of the Ox radicals, the HOx radicals, and the nitrogen species at the sampling points. The calculations make use of the measurements from radiometers to scale clear sky photolysis rates to account for cloud cover and ground albedo at the sampling time/point. The concentrations of the nitrogen species in each of the sampled air parcels are computed assuming they are in instantaneous equilibrium with the measured NO and O_3. The diurnally varying species concentrations are next calculated using the box model and used to estimate the diurnally averaged production and removal rates of ozone for the sampled air parcels. Clear sky photolysis rates are used in the diurnal calculations. The campaign also provided measured concentration of NO_y. The observed NO/NO_y ratio is usually larger than the model calculated equilibrium value. There are several possible explanations. It could be a result of recent injection of NO into the air parcel, recent removal of HNO_3 from the parcel, recent rapid transport of an air parcel from another location, or a combination of all processes. Our analyses suggest that the local production rate of O_3 can be used as another indicator of recent NO injection. However, more direct studies using air trajectory analyses and other collaborative evidences are needed to ascertain the roles played by individual process. *INDEX TERMS:* 0365 Atmospheric Composition and Structure: Troposphere—composition and chemistry; 0368 Atmospheric Composition and Structure: Troposphere—constituent transport and chemistry; 0322 Atmospheric Composition and Structure: Constituent sources and sinks; 0345 Atmospheric Composition and Structure: Pollution—urban and regional (0305); *KEYWORDS:* tropospheric ozone, biomass burning, lightning

Citation: Ko, M., W. Hu, J. M. Rodríguez, Y. Kondo, M. Koike, K. Kita, S. Kawakami, D. Blake, S. Liu, and T. Ogawa, Photochemical ozone budget during the BIBLE A and B campaigns, *J. Geophys. Res.*, *107*, 8404, doi:10.1029/2001JD000800, 2002. [printed *108*(D3), 2003]

1. Introduction

[2] The two phases of the BIBLE (Biomass Burning and Lightning Experiment) campaign carried out during September–October of 1998 (BIBLE A) and August–September of 1999 (BIBLE B) were designed to study tropospheric ozone chemistry in tropical Asia [see *Kondo et al.*, 2002a, 2002b]. The instruments provide measured concentrations of NO, NO_y, O_3, H_2O, CO, CH_4, NMHCs, several methyl halides and alkyl nitrates, as well as radiometer measurements that provide information on in situ photolysis rates. These data have been compiled by the BIBLE Science team into 1-min merged files for each flight. The merged files provide concentrations of trace gases at the sampling point along the flight track. They provide sufficient constraints (with some additional assumptions) to allow a photochemical model to calculate concentrations of radical species. The calculated radical concentrations can then be used to compute the instantaneous production and removal rates of ozone.

[3] The measured concentrations do not provide sufficient constraints to give unique values for the ozone production and removal rates. Different assumptions would lead to different values [*Davis et al.*, 1996; *Jacob et al.*, 1996; *Folkins et al.*, 1997; *Jaegle et al.*, 1998]. One aim of the campaign is to examine the role lightning and/or biomass burning play in the reactive nitrogen budget [*Price et al.*, 1997; *Liu et al.*, 1999; *Levy et al.*, 1999; *Galanter et al.*, 2000] and how that affects the ozone budget. In this

[1]Atmospheric and Environmental Research, Inc., Lexington, Massachusetts, USA.
[2]Now at NASA Langley Research Center, Hampton, Virginia, USA.
[3]Now at Virginia Department of Environmental Quality, Richmond, Virginia, USA.
[4]Rosenstiel School of Marine and Atmospheric Science, University of Miami, Miami, Florida, USA.
[5]Research Center for Advanced Science and Technology, University of Tokyo, Tokyo, Japan.
[6]Department of Earth and Planetary Sciences, University of Tokyo, Tokyo, Japan.
[7]National Space Development Agency of Japan, Earth Observation Research Center, Tokyo, Japan.
[8]Chemistry Department, University of California, Irvine, California, USA.
[9]Institute of Earth Sciences, Academia Sinica, Taipei, Taiwan.

0148-0227/02/2001JD000800$09.00

paper, we compare the model calculated [NO]/[NO_y] ratio with the observed [NO]/[NO_y] ratio, and use this along with the model calculated ozone production rate to obtain an indicator for the time elapsed since previous perturbation to the nitrogen species. (We will use [X] to denote the concentration of X.) This is the reason why we chose to use measured [NO] in our calculations and compare the model calculated [NO_y] with the observed values of [NO_y]. Section 2 discusses the overall philosophy of our approach. The model descriptions, the calculation procedures and model results are given in sections 3, 4 and 5.

2. Approach

2.1. Process Model and Aircraft Data

[4] The interactions between model and measurements take on many levels of complexity. In theory, if one has the correct chemical mechanisms and transport rates built into a model, one would only need detailed emissions histories of the source gases to simulate all the trace species for comparison with measured values. This point-by-point validation cannot be achieved in practice for many reasons. There is no independent way of verifying that the adopted photochemical scheme is complete. One cannot be sure that the emission histories and transport rates are sufficiently accurate to account for small local variations. Thus, when discrepancies occur, it is seldom possible to attribute them to a specific cause.

[5] A process model assigns values to concentrations of certain species and calculates the concentrations for a subset of the species to test specific processes. The most common of these is the photochemical box model. The approach takes advantage of the fact that certain species have photochemical lifetimes on the order of minutes and shorter. Thus, if the concentrations of all other species are given, the concentrations of the short-lived species are determined by the local solar insolation at the time of the measurement. In practice, the situation is less than ideal because concentrations of some species with intermediate lifetimes (of order days) are not measured.

2.2. Ozone Production and Removal Rates

[6] Current understanding of ozone chemistry shows that the production and removal rates of ozone in the troposphere are dominated by HO_x and NO_x chemistry [see, e.g., *Davis et al.*, 1996; *Crawford et al.*, 1997a, 1997b; *Klonecki and Levy*, 1997]:

$$P = [NO] \times \{k_{NO+HO_2}[HO_2] + k_{NO+CH_3O_2}[CH_3O_2] + k_{NO+RO_2}[RO_2]\} + \ldots$$
$$L = [O_3] \times \left\{ k_{HO_2+O_3}[HO_2] + k_{OH+O_3}[OH] + k_{O(^1D)+H_2O}[H_2O] \cdot \frac{O(^1D)}{[O_3]} + \ldots \right\} \quad (1)$$

In order to calculate the instantaneous production and removal rates of ozone, we must obtain values for [NO], [HO_2], [OH], [$O(^1D)$], and various [RO_2]s. Many of the aircraft measurement campaigns were designed to provide measured concentrations of enough species so that the ozone production and removal rates can be obtained from a constrained photochemical model. Examples of previous studies include those by *Wennberg et al.* [1994] and *Fahey et al.* [2000] for the stratosphere and *Jacob et al.* [1996], *Folkins et al.* [1997], *Crawford et al.* [1997a, 1997b], *Jaegle et al.* [1998], and *Schultz et al.* [1999] for the troposphere. In the BIBLE campaign, the concentration of NO was available from the NO instrument [*Kondo et al.*, 2002a, 2002b]. Since O_3 is measured, [O^1D] can be calculated assuming photochemical equilibrium using information from the radiometer measurements; this leaves [OH], [HO_2], and other [RO_2]s.

[7] The study of HOx has been a focus of a series of aircraft campaigns organized by NASA's GTE program. Prior to the availability of OH and HO_2 measurements, process models were used to calculate the concentrations of OH and HO_2 [*Kotamarthi et al.*, 1997; *Crawford et al.*, 1999; *Jaegle et al.*, 2001]. The ATHOS instrument [*Brune et al.*, 1998] aboard the DC-8 during the SUCCESS campaign provided in situ airborne measured concentrations of OH and HO_2 in the troposphere. The instrument was also deployed during the PEM Tropics-B campaign in 1999 [*Brune et al.*, 1999]. The data have been used in a number of studies for comparisons with model predicted concentrations. Analyses using the PEM Tropics-B data show that the model predicted median concentrations are within 15% of the measured median values if measured values of [H_2O_2] and [CH_3OOH] are used in the calculation. There is no direct way to verify model calculated concentrations of RO_2 radicals at this point. Calculations will be performed assuming RO_2s are in photochemical equilibrium with the NMHC precursors.

[8] Because the radical concentrations in Equation (1) vary with solar zenith angle (SZA), the instantaneous production and loss rates for ozone are also a strong function of SZA. The measurements along the flight tracks were made at various SZAs. For the purpose of identifying how different compositions in an air parcel may affect production and loss rates, it is more useful to use diurnal averaged rates. Strictly speaking, the diurnal rates associated with the sampled air parcel should be calculated using the history (location and solar exposure) of the air parcel following the back trajectory. In practice, there are certain difficulties associated with this. One of these is the lack of information on cloud cover and/or change in albedo along the trajectory. The other is finding the appropriate concentrations to initialize the concentrations in the air parcel. Our approach (to be discussed in section 4) assumes that the air parcel is in photochemical equilibrium with the measured concentrations of O_3, H_2O, CO, CH_4, NMHCs, and the concentration of NO_x constrained by observations. Our analyses show that, once the model adopts the measured [NO], the model calculated [OH], [HO_2], and the production and removal rates for ozone are not very sensitive to how the other nitrogen species are calculated.

2.3. NO_y Partitioning and Recent NO Injection

[9] The measured [NO_y] were not used directly in our calculations. Instead, we used the measured [NO] and calculated the concentrations for HNO_3 and other nitrogen species assuming that all the nitrogen species are in photochemical equilibrium. This is similar to the approach adopted by *Kiem et al.* [1999]. If there have been recent injections of NO (from

a biomass burning source or from lightning) in the air parcel, the nitrogen species would not be in equilibrium. Our purpose is to compare the model calculated [NO_y] with the observed values and to use the results of the comparison as a partial indicator for whether there have been recent injections of NO for that air parcel. Several things complicate the interpretation of the comparison. The larger measured [NO]/[NO_y] ratio may have been due to recent scavenging of HNO_3. Furthermore, the troposphere is not static. An air parcel sampled at a particular location may not have been at that location for sufficient time to attain equilibrium corresponding to the local conditions. This argues against using comparison of measured and model calculated [NO_y] as the sole criteria. We propose that the production rate of ozone (in percent per day) would provide additional clues on whether recent injection of NO has occurred.

3. Point Model Calculations

3.1. Model Description

[10] The AER photochemical box model [*Kotamarthi et al.*, 1997] was used to simulate the concentrations of the radical species along the flight tracks. There are 93 species in the box model including the O_x, HO_x, NO_x, Cl_Y and Br_Y families. It includes explicit degradation schemes for CH_4 and C_2H_6 and higher-order NMHCs schemes according to *McKeen et al.* [1991]. The reaction rate constants were updated according to JPL-97 [*DeMore et al.*, 1997].

[11] In the calculations, concentrations of the long-lived species O_3, H_2O, CH_4, CO, and NMHCs were constrained by the 1-min merged files. In addition, the concentration of NO was also taken from the merged file and fixed at the observed value. In light of the importance of acetone in the HOx budget [see, e.g., *Singh et al.*, 1995], we fixed the concentration of acetone using the correlation between acetone and CO derived from the PEM-West B data [*McKeen et al.*, 1997]. We deemed this to be reasonable given that the BIBLE campaign and PEM-West-B were over similar geographical regions. Neither H_2O_2 nor CH_3OOH were measured in the campaign. Their concentrations were calculated assuming local photochemical equilibrium. We ignored halogen chemistry in the calculation by setting the concentrations of Cl_Y and Br_Y equal to zero. We also ignored heterogeneous chemistry. The heterogeneous reaction of $N_2O_5 + H_2O$ producing HNO_3 would have changed the nitrogen partitioning with appreciable effects particularly during winter at high latitudes. Because we fixed [NO] in our calculation, including the reaction would change only [HNO_3] and other nitrogen species. Analysis of the HO_x budget would show that the concentration of HNO_3 has a small effect on the calculated concentrations of OH and HO_2. The other reactions (such as $BrONO_2 + H_2O$) could also affect the HO_x budget. Sensitivity calculations performed using typical values of Cl_Y and Br_Y show that the effect on the ozone production and removal rates is small.

[12] The point model provided $\{n_j^{t_{obs}}\}$, which is the set of concentrations for species that were obtained by solving the system of instantaneous equilibrium v

$$P_i\left(\left\{n_j^{t_{obs}}\right\}, SZA(t_{obs})\right) = L_i\left(\left\{n_j^{t_{obs}}\right\}, SZA(t_{obs})\right) n_i^{t_{obs}} \qquad (2)$$

where $n_i^{t_{obs}}$ (molecules/cm^{-3}) is the concentration of the ith species, P_i (molecules/cm^{-3} s^{-1}) and L_i (s^{-1}) are the respective production and removal frequency and are functions of other species concentrations and the solar zenith angle at the time of observation ($SZA(t_{obs})$). Species calculated this way included O, O(^{3}P), O(^{1}D), OH, HO_2, H_2O_2, CH_3O_2, NO_2, PAN, HNO_3, NO_3, HNO_4, N_2O_5, HONO, CH_3OOH, C_2H_5OOH, CH_3CHO, CH_3CO_3, CH_3CO_3H, $C_2H_2O_2NO_2$. The point-by-point calculation was performed only for sampling points at solar zenith angles less than 60° so that the equilibrium criteria are better met.

3.2. Scaling of Photolysis Rates

[13] Two photolysis rates ($J(NO_2 \rightarrow NO)$ and $J(O_3 \rightarrow O(^1D))$) were derived from filter radiometer measurements [see *Kita et al.*, 2002]. The absolute calibration factor for $J(NO_2 \rightarrow NO)$ was provided by the manufacturer. For $J(O_3 \rightarrow O(^1D))$, Kita et al. used the correlation between the measured radiance and the derived photolysis rate from the PEM-Tropics-A campaign to obtain the photolysis rate. Two scaling factors were defined as the ratio of the derived photolysis rate and the model calculated clear sky photolysis rate ($R_{O(^1D)}$) for $J(O_3 \rightarrow O(^1D))$ and R_{NO_2} for $J(NO_2 \rightarrow NO)$. These factors were used to scale model calculated clear sky photolysis rates to simulate cloud effect. $R_{O(^1D)}$ was used for absorbers with cross-section peaking near 300 nm while R_{NO_2} was used for those peaking near 400 nm. Figure 1 shows several examples of how the ratios varied along the flight track from flight 3, flight 8, flight 9, and flight 13. (For location of the flight tracks, see Figures 1 and 2 of *Kondo et al.* [2002a].) Note that values at landing usually show anomaly. In addition, the values for the latter third of flight 13 are for SZA close to 60° (see Figure 2). The rest of the behavior is typical although the magnitude of the scaling factor is on the large side compared to other flights in the same campaign. In all cases, the ratio was close to unity around 4–6 km. Above this altitude, the ratio was usually larger than 1, indicating the effect of reflection from cloud below the flight track. Below 4 km, the ratio was more likely to be less than 1, indicative of clouds overhead.

3.3. Constrained Parameters

[14] The different panels from Figure 2 summarize the key measured data from the merged file that were used in the calculations. Data from flight 3, flight 6, and flight 13 shown in Figure 2a were taken over open ocean. Data from flight 8, flight 9, and flight 11 shown in Figure 2b correspond to flights out of Bandung. Note that the individual panel does not necessarily use the same scale. The top panels show the flight altitude, SZA, and [H_2O]. The measured concentrations of NO and O_3 are shown in the middle panels. The measured concentrations of CO and the NMHCs are shown in the bottom panel. Note that the NMHC data are interpolated from 5-min averages.

3.4. Model Calculated $n_{OH}^{t_{obs}}$ and $n_{HO_2}^{t_{obs}}$

[15] Without direct measurements of OH and HO_2 in the campaigns, there is no easy way to verify whether the assumptions made in the calculations (concentration of acetone; equilibrium assumptions for H_2O_2, and CH_3OOH; photolysis scale factors) are appropriate. The same model

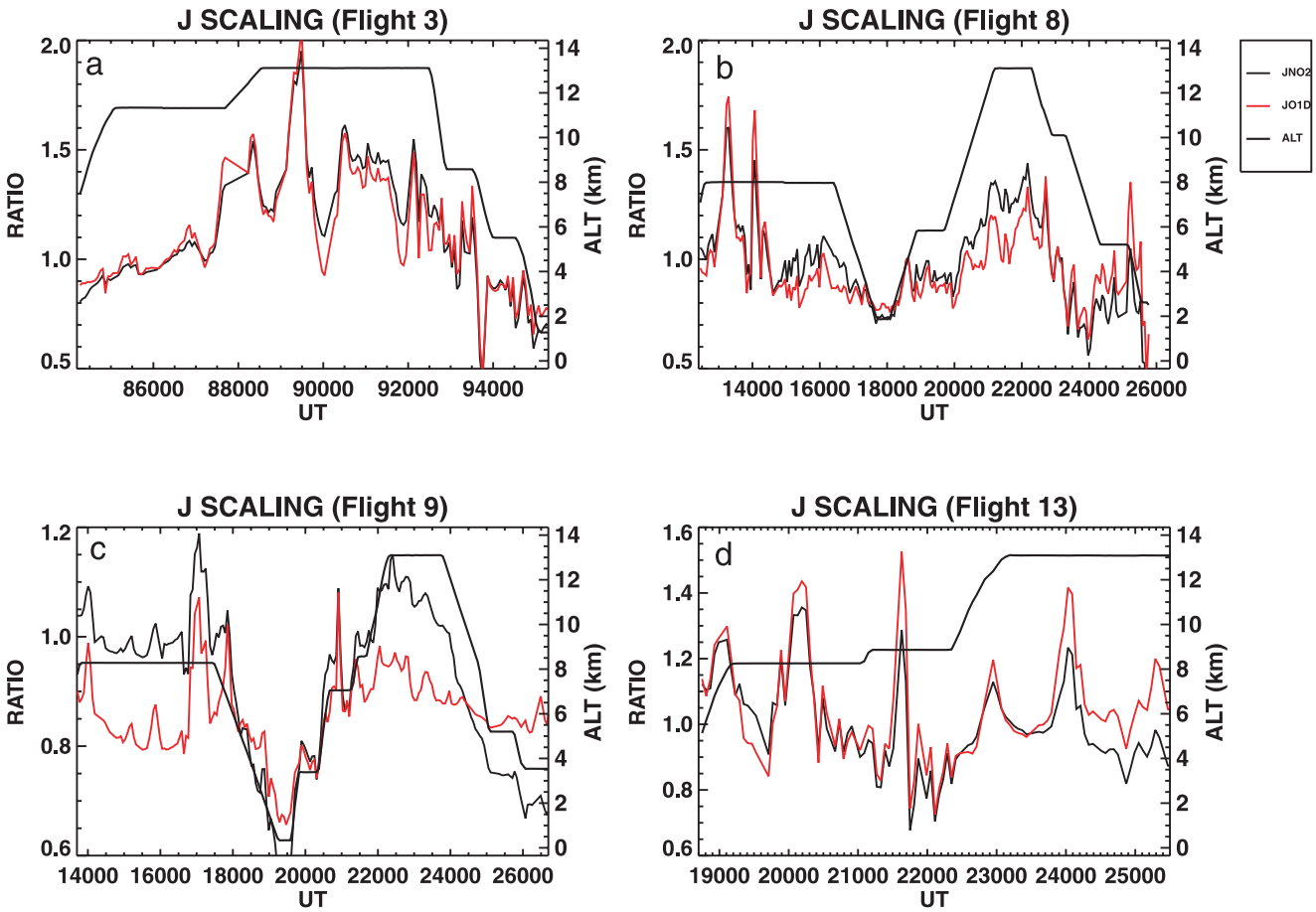

Figure 1. Scaling factor for photolysis rates for (a) flight 3, (b) flight 8, (c) flight 9, and (d) flight 13 from BIBLE A. Values plotted are ratios of the observed rate for photolysis of O_3 to produce $O(^1D)$ to the clear sky rate ($R_{O(^1D)}$, red curve) and ratios for photolysis of NO_2 (R_{NO_2}, black curve). The altitude of the flight track is given by the thick black curve.

was used to analyze data from PEM Tropics-B. With H_2O_2 and CH_3OOH fixed at the observed values, the model calculated median concentrations of OH and HO_2 were within 15% of the measurements. The calculated values for OH and HO_2 also accounted for about 70% and 90% of the observed variance respectively. Sensitivity analyses using the PEM Tropics-B data show that the calculated OH and HO_2 would be 20% larger when H_2O_2 and CH_3OOH are calculated assuming photochemical equilibrium.

[16] Examination of the budget indicated that the production of HOx is dominated by the reaction of $O(^1D)$ with H_2O below 8 km. Above 8 km, photolysis of H_2O_2, photolysis of CH_2O, and the reaction of CH_3O_2 with NO play comparable roles. Below 5 km, the removal of HO_x results from equal contributions from the reaction of OH with CH_4, the self reaction of HO_2 forming H_2O_2, and the reaction of CH_3O_2 with HO_2. The first two reactions continue to play an important role above 5 km, while the third becomes less important with the reaction of OH with HO_2 playing an increasing role. The partitioning between OH and HO_2 is controlled by NO, O_3, and CO. Below 6 km, the local concentration of OH is determined by the balance between production from $O(^1D) + H_2O$, and the removal by reaction with CO. Above 8 km, production of OH is dominated by the reaction of HO_2 with NO while the removal by reaction with CO continues to be key. The production of HO_2 is dominated by the reaction of OH + CO in the troposphere. The removal is dominated by reaction with NO at high altitudes and by the reaction with CH_3O_2 and the formation of H_2O_2 at low altitudes. Thus the budget analyses suggest that once the observed NO con-

Figure 2. (opposite) Plots showing measured concentrations that are used to constrain the photochemical box model. Data from six flights from BIBLE A are shown. Flights 3, 6, and 13 in Figure 2a are over open ocean, while flights 8, 9, and 11 in Figure 2b are survey flights from Bandung. Note that the panels for different flights on the same row may have different scales. (top) Altitude of flight track (thick black) in kilometers, local solar zenith angle (black) in degrees, and measured H_2O (red) in mole fraction on a log scale. (middle) Measured mixing ratios of O_3 (thick) in ppbv and measured mixing ratio of NO (thin) in pptv. (bottom) Measured mixing ratios of CO in ppbv, mixing ratios of the NMHCs are in pptv. The plotted values for C_2H_6 correspond to the measured values divided by 10. NMHC are interpolated from 5-min measurements.

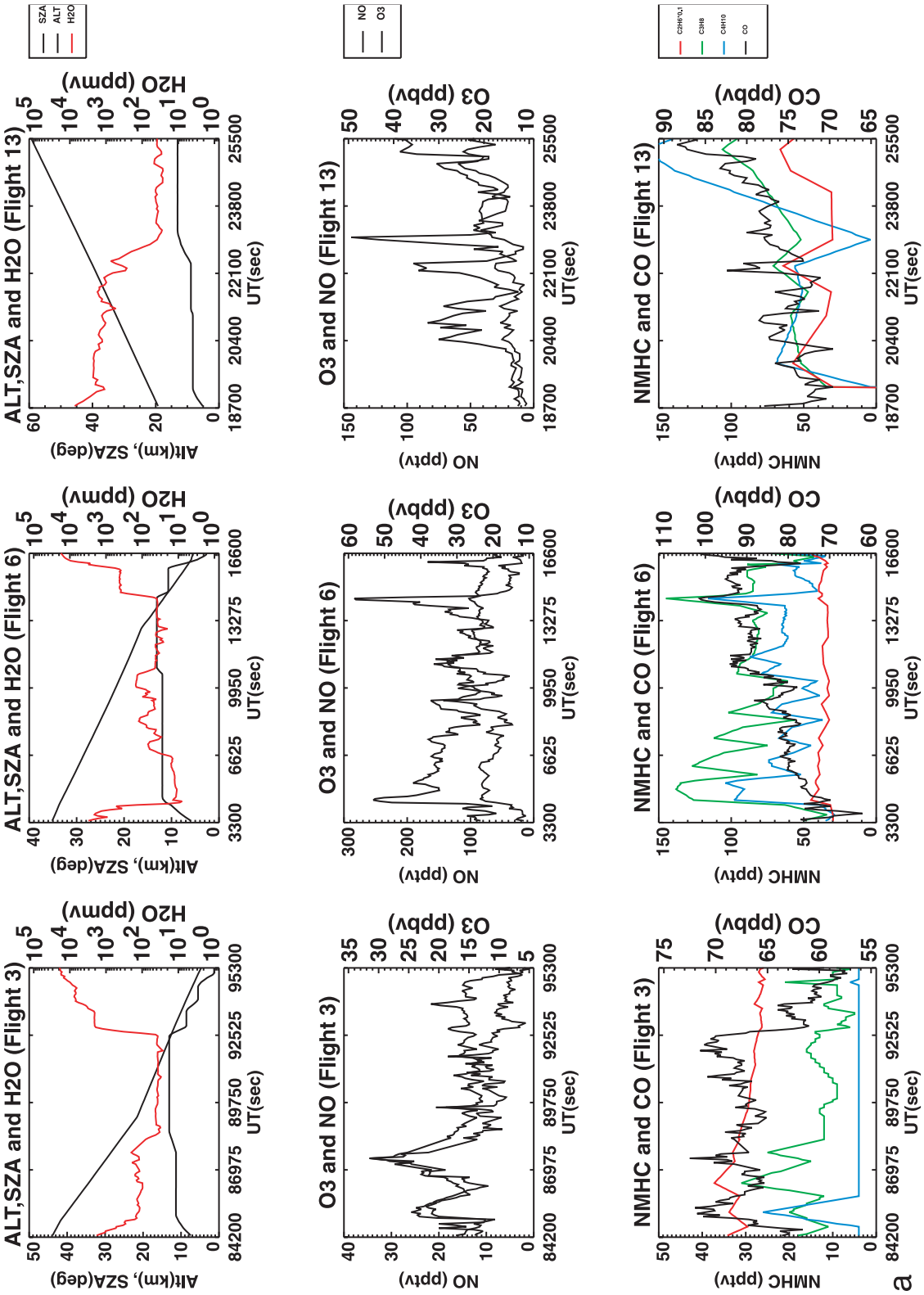
ALT,SZA and H2O (Flight 3)
Alt(km), SZA(deg)
H2O (ppmv)
UT(sec)
O3 and NO (Flight 3)
NO (pptv)
O3 (ppbv)
NMHC and CO (Flight 3)
NMHC (pptv)
CO (ppbv)
ALT,SZA and H2O (Flight 6)
O3 and NO (Flight 6)
NMHC and CO (Flight 6)
ALT,SZA and H2O (Flight 13)
O3 and NO (Flight 13)
NMHC and CO (Flight 13)
SZA
ALT
H2O
NO
O3
C2H6,O,I
C3H8
C4H10
CO
a

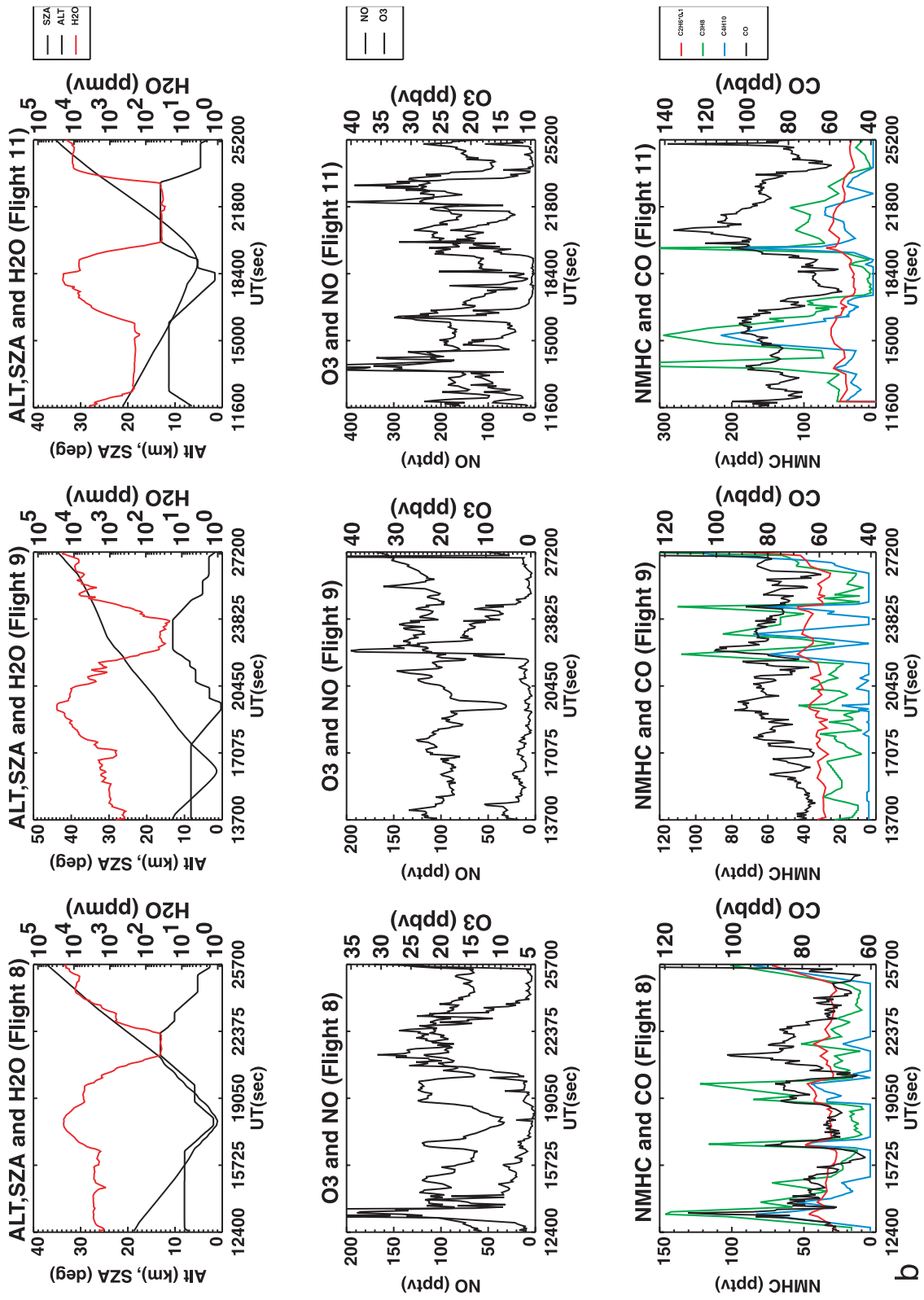

Figure 2. (continued)

centration is used in the computation, the results are not very sensitive to how the other NO_y species are determined. Clearly, the results will be better constrained if measured values are available for H_2O_2 and CH_3O_2. The calculated values for $n_{OH}^{t_{obs}}$ and $n_{HO_2}^{t_{obs}}$ along the flight tracks for selected flights are shown in the first row of Figure 3.

4. Diurnal Averaged Production and Removal Rates for Ozone

4.1. Method

[17] The results from the point model ($\{n_j^{t_{obs}}\}$) provide the instantaneous equilibrium concentrations of the species at local time at the sampling point. In the real atmosphere, some of the species are not in equilibrium because their lifetimes are of order days. There are several ways one can account for the diurnal variations of those species and obtain diurnal averaged ozone production and removal rates. One way is to use the results from the point model as initial values for the diurnal box model and simulate the diurnal behavior of the radical species assuming the air parcel is stationery at the same spatial position. The results will depend on the treatment of cloud cover. The decision has to be made whether to assume the same cloud cover that occurs at the sampling point persists over several days, or to assume a climatological cloud cover, or to use clear sky photolysis rates. We chose to perform the calculation using clear sky photolysis rates since it is unlikely that the same cloud cover at the sampling time would have persisted over the several previous days.

[18] We used the model to propagate the initial values ($n_j^{t_{obs}}$) by solving

$$\frac{\partial n_i(t)}{\partial t} = P_i(t, n_k(t)) - L_i\big(t, n_{k\neq i}(t)\big) n_i(t) \tag{3}$$

for O, O(^{3}P), O(^{1}D), OH, HO_2, H_2O_2, CH_3OOH, CH_3O_2, NO, NO_2, PAN, HNO_3, $CH_3O_2NO_2$, NO_3, HNO_4, N_2O_5, HONO, C_2H_5OOH, CH_3CHO, CH_3CO_3, CH_3CO_3H, $C_2H_2O_2NO_2$, and acetone. The concentrations for O_3, H_2O, CH_4, CO, and NMHCs were held fixed and assumed not to change with SZA. We chose not to include any external source or sink term for the NO_y species in equation (3). As a result [NO_y] is preserved, i.e. $n_{NO_y} = n_{NO_y}^{t_{obs}}$. Since $n_i^{t_{obs}}$ $n_i^{t_{obs}}$ are in instantaneous equilibrium at the sampling points with adjusted photolysis rates, $n_i(t_{obs})$ calculated using clear-sky photolysis rates may no longer equal $n_i^{t_{obs}}$ after a 1-day propagation. Thus some adjustment has to be made if we wish to continue to use the measured NO concentration to constrain the model results. We run the model for 20 days so that NO_x = NO + NO_2 is in approximate diurnal equilibrium with NO_y. It is difficult to obtain exact diurnal equilibrium between NOx and NO_y because of a slow conversion between NO_x and HNO_3 due to weak feedback on OH. We then scaled the NO_y species by the NOx concentrations

$$n_k^*(t) = n_k(t) \times \frac{n_{NO}^{t_{obs}} + n_{NO_2}^{t_{obs}}}{n_{NO}(t_{obs}) + n_{NO_2}(t_{obs})} \tag{4}$$

where $\{n_k(t)\}$ consists of NO, NO_2, NO_3, HNO_4, N_2O_5, PAN, HNO_3, and $CH_3O_2NO_2$. The rest of the species were unchanged. The scaling assumes that the NO_y species are in equilibrium with [NO_x] = [NO] + [NO_2] at the time of observation where we used the measured $J(NO_2 \rightarrow NO)$ to account for the effect of cloud cover on the partitioning between NO and NO_2 at the time of observation. Our results show that the majority of the sampling points has $n_{NO_y}^*(t) > n_{NO_y}^{t_{obs}}$. Finally, we propagate the solution for 1 more diurnal cycle to obtain all the species $\{n_j^{II}(t)\}$ that will be used to calculate the production and removal rates of ozone. Note that the measured $J(O_3 \rightarrow O(^1D))$ values were not used in the diurnal calculation.

[19] As discussed in section 1, other methods for computing the diurnal behavior are equally valid. An alternate method would be to adjust $n_{NO}(t_{obs}) + n_{NO_2}(t_{obs})$ after each 24-hour propagation to equal $n_{NO}^{t_{obs}} + n_{NO_2}^{t_{obs}}$. An upward (downward) adjustment can be interpreted as an external source (sink) for NO_x in the model. One would have to choose whether to make the adjustment at one instance in time or spread the production/removal over a 24-hour period. However, if one runs the model for several days to achieve approximate diurnal equilibrium, the results should be similar to our method as long as the equilibrium NO_x/NO_y ratio is not very sensitive to NO_y concentration.

4.2. Results

[20] The calculated values for $n_{OH}^{II}(t_{obs})$ and $n_{HO_2}^{II}(t_{obs})$ along the flight tracks are shown in Figure 3 along with $n_{OH}^{t_{obs}}$ and $n_{HO_2}^{t_{obs}}$. At most altitudes, the differences between the point model values and the diurnal model values are largely due to the clear-sky (in the diurnal model) versus adjusted photolysis rates (in the point model) in the calculations. The differences above 12 km are particularly large, approaching a factor of 2 (see flights 3 and 13). At those altitudes, the model calculated concentrations of $CH_3O_2NO_2$ are large and the model calculated NO_y is much larger than the observed NO_y. We will explore this in future studies.

[21] The concentrations $\{n_j^{II}(t)\}$ were used in the expression in equation (1) to calculate the diurnally average production rate ($\langle P \rangle$) and removal rate ($\langle L \rangle$) for ozone. A sample of the results is shown in the second row in Figure 3. The calculated mean and median values are plotted in Figures 4 and 5 for BIBLE A and BIBLE B, respectively. In each case, we sorted the data that satisfy the solar zenith angle criteria by altitude and computed the mean and median values for each altitude. The standard deviations and the percentiles are given in the corresponding figures as indicators of the spread of the values. The difference between the median and the mean values provide an indication of the distribution. The mean production value is typically 1.5 times the median production value, suggesting that the distribution is skewed toward larger values. In contrast, the mean removal rate is only 10% larger than the median values. This is consistent with the fact that the production term depends more directly on NO concentrations which show large variability. For BIBLE A, the median net value is negative below 7 km. The altitude behavior of the net tendency in BIBLE A is similar to results calculated by *Crawford et al.* [1997a] for the tropics corresponding to the "high NOx" regime that are influenced by continental outflow. The tendency is positive above 6–8 km and negative below. Similar behavior was calculated using data from the tropical South Atlantic

during Trace-A [*Jacob et al.*, 1996], from the tropical North Pacific during PEM-West A [*Davis et al.*, 1996a], from the tropical South Pacific during PEM-Tropics A [*Schultz et al.*, 1999]. The median net ozone tendency is positive below 3 km in BIBLE B because most of the data were obtained over Australia where the effects from bio-mass burning are large [*Takegawa et al.*, 2002].

[22] The integrated column mean and median values (from 1 km to 14 km) are given in Table 1. The data below 1 km is excluded because most of them were taken during take-offs and landings. We divided the data into three sets, representing the Ferry flight north of the equator, flights over Indonesia between the equator and 10S, and flights over Australia south of 10S. Model results based on GCM simulations [*Levy et al.*, 1999] reported that the tendency term due to chemistry in the tropical free troposphere is +163 Tg O3/yr. This is equivalent to $+4 \times 10^{10}$ molecules/cm^2/s. *Crawford et al.* [1997a] reported values of $+0.1 \times 10^{10}$ molecules/cm^2/s and -20×10^{10} molecules/cm^2/s for the "high NO_x" and the "low NO_x" regimes respectively. *Schultz et al.* [1999] calculated -18.4×10^{10} molecules/cm^2/s using data from PEM-Tropics A for the tropics. Clearly, the calculated integrated tendency is sensitive to the NO_x concentrations in the air sampled in each study. The value given by Levy et al. applies to the whole troposphere and includes regions with high NO_x and large ozone production. In contrast, the Crawford et al. and Schultz et al. studies used data from remote regions where ozone removal dominates.

4.3. Uncertainties Associated With the Method

[23] *Crawford et al.* [1997b] provided expressions for diurnal averaged ozone production and removal rates.

$$\langle P\rangle_{Crawford} = 2.19 \times 10^7 [NO] \sqrt{\frac{[H_2O][O_3]\cos(\theta_{HN})}{[M]TOMS}} \quad \text{(ppbv/day)}$$

$$\langle L\rangle_{Crawford} = 0.103 \times \frac{[O_3][H_2O]^{0.6}\cos(\theta_{HN})}{TOMS} \quad \text{(ppbv/day)}$$

where [NO] is in pptv, [H_2O] in ppmv, [O_3] in ppbv, [M] is the air density in molecule/cm^3, θ_{HN} is the noon-time SZA, TOMS is the overhead ozone column in Dobson units. The numerical parameters were from *Crawford et al.* [1997b] who obtained them from a fit of their diurnal model results performed for extra-tropical data in late winter and early spring from PEM-West B below 12 km. Based on the PEM-West B data, *Crawford et al.* [1997a, 1997b] chose averaged cloud-correction factors for their photochemical model. The chosen values ranged between 0.8 and 1.0 below 5 km and between 1.0 and 1.18 above 5 km for the extratropics [*Crawford et al.*, 1997b]. In their calculations, all photolysis rates were multiplied by the same cloud correction factors that were specified as functions of altitude. We compared our values for $\langle P\rangle$ and $\langle L\rangle$ for BIBLE A with the values calculated using equation (5) in Figure 6. Points for $\langle P\rangle$ are typically within 50%. The points that differ for more than a factor of 2 are from around 10 km where [NO] is around 400 pptv and [H_2O] is around 200 ppmv. With these concentrations, [HO_2] depends on [NO] and can no longer be parameterized using [H_2O] and [O_3]. Our values for $\langle L\rangle$ are a factor of 2 larger than values calculated using equation (5).

[24] Figures 7 and 8 show the percent contributions of the various terms that make up the production ($\langle P\rangle$) and removal ($\langle L\rangle$) rates of ozone. With the assumptions we made, the model results show that the reaction HO_2 + NO constitutes 60%–80% of $\langle P\rangle$, with CH_3O_2 + NO contributing the remaining 20%–40%. The next term is from the photolysis of O_2, which is minimal. Contribution from RO_2 reaction is at most a few percent from a few sampling points with unusually large NMHC concentrations. The $\langle L\rangle$ term is dominated by the reaction of $O(^1D)$ + H_2O in the lower troposphere, responsible for 80%. The reactions of O_3+ HO_2 and O_3 + OH make up the rest. In the upper troposphere, the reactions of the HOx radicals with O_3 add to 80%, with the $O(^1D)$ reaction contributing 20%.

[25] We now examine how the assumptions adopted in our calculations may affect the calculated production and removal rates for ozone. The first is the assumption that the nitrogen species are in equilibrium with the observed [NO]. The question can be raised how this assumption affects the model calculated [OH] and [HO_2], and how they in turn affect the ozone production and removal rates. As pointed out in section 3.5, the model calculated [OH] and [HO_2] are not very sensitive to this assumption as long as observed [NO] is used in the calculations. As discussed in section 3.4, we estimated that the [OH] and [HO_2] should be within 50% of the actual values.

[26] The second assumption has to do with using clear sky photolysis rates for the diurnal calculations. The information on the derived $J(NO_2 \rightarrow NO)$ was used in the NOx scaling in equation (4) at the sampling point. The information on the derived $J(O_3 \rightarrow O(^1D))$ was not used. Had we used an average cloud correction factor with values between 0.8 and 1.2 similar to *Crawford et al.* [1997b], the $\langle P\rangle$ and $\langle L\rangle$ values would be smaller by about 10%. Finally, we do not have reliable information to estimate the uncertainty in CH_3O_2. However, the budget analysis showed that the CH_3O_2 term should contribute up to 50% (Figure 7). Thus we estimate that $\langle P\rangle$ should be within a

Figure 3. (opposite) Plots showing calculated results from the point model and the diurnal model. Data from six flights from BIBLE A are shown. Flights 3, 6, and 13 (Figure 3a) are over open ocean, while flights 8, 9, and 11 (Figure 3b) are survey flights from Bandung. Note that the panels for different flights on the same row may have different scales. (top) Model calculated local concentrations (molecules cm^{-3}) for OH and HO_2 from the point model ($n_{OH}^{t_{obs}}$(thin black) and $n_{HO_2}^{t_{obs}}$ (thick black)) and the diurnal model ($n_{OH}^{II}(t_{obs})$ (thin red) and $n_{HO_2}^{t_{obs}}$(thick red)) along the flight track. (middle) Model calculated ozone production rate (black), ozone removal rate (pink), and ozone net production rate (blue) in units of percent per day. The altitude along the flight track is also included. (bottom) The color stack plot shows the contributions (pptv) from each nitrogen species to the model calculated NO_y. The value for [NO] is constrained to be the observed value. The thick blue line is the measured [NO_y]. The thin blue line is the parameter $Frac = 1 - \frac{[NO_y]_{meas}}{[NO_y]_{equil}}$.

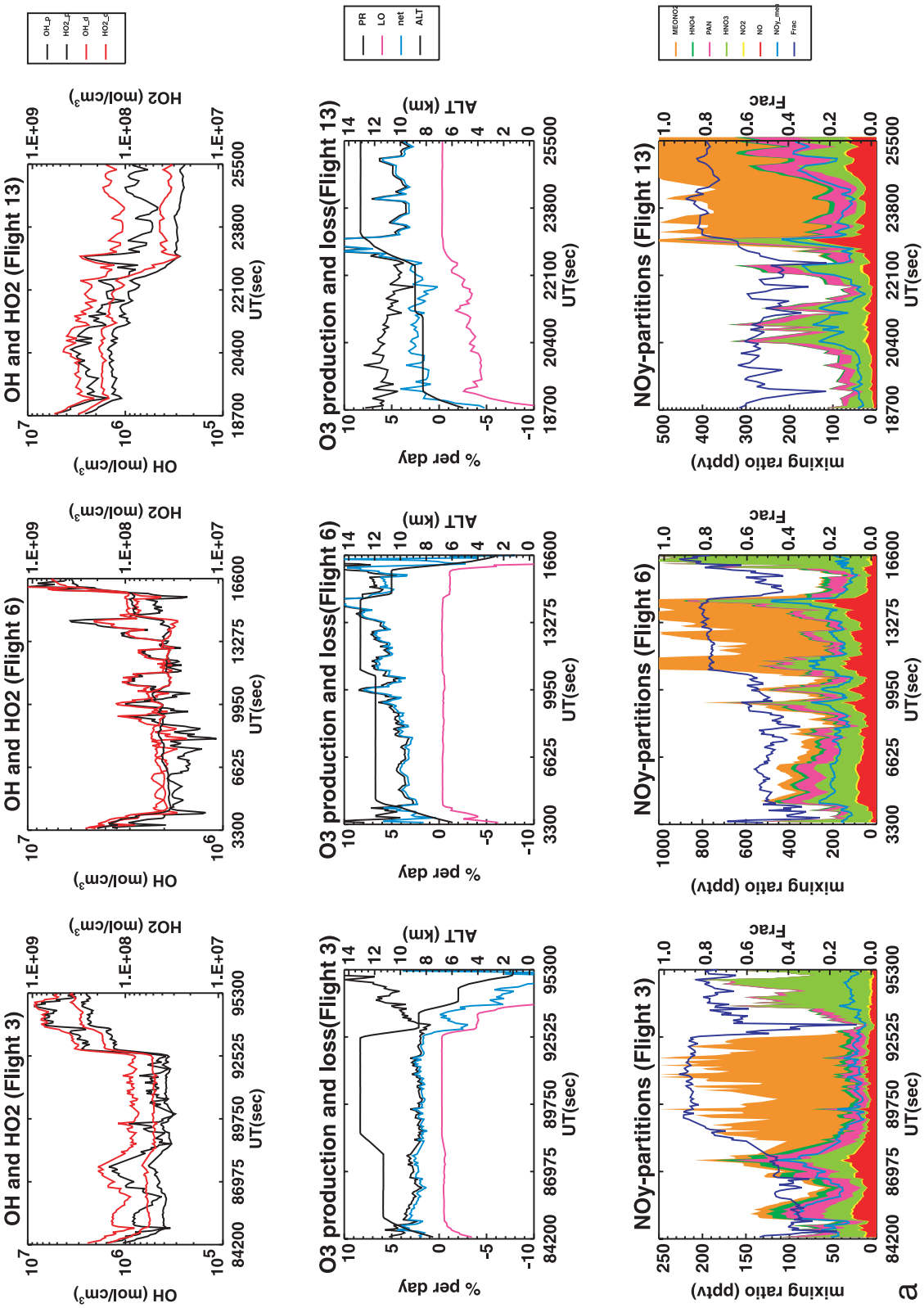
OH and HO2 (Flight 3)
OH (mol/cm3)
HO2 (mol/cm3)
UT(sec)
O3 production and loss(Flight 3)
% per day
ALT (km)
PR
LO
net
ALT
NOy-partitions (Flight 3)
mixing ratio (pptv)
Frac
MEONO2
HNO4
PAN
HNO3
NO2
NO
NOy_mea
Frac
OH and HO2 (Flight 6)
O3 production and loss(Flight 6)
NOy-partitions (Flight 6)
OH and HO2 (Flight 13)
O3 production and loss(Flight 13)
NOy-partitions (Flight 13)
a

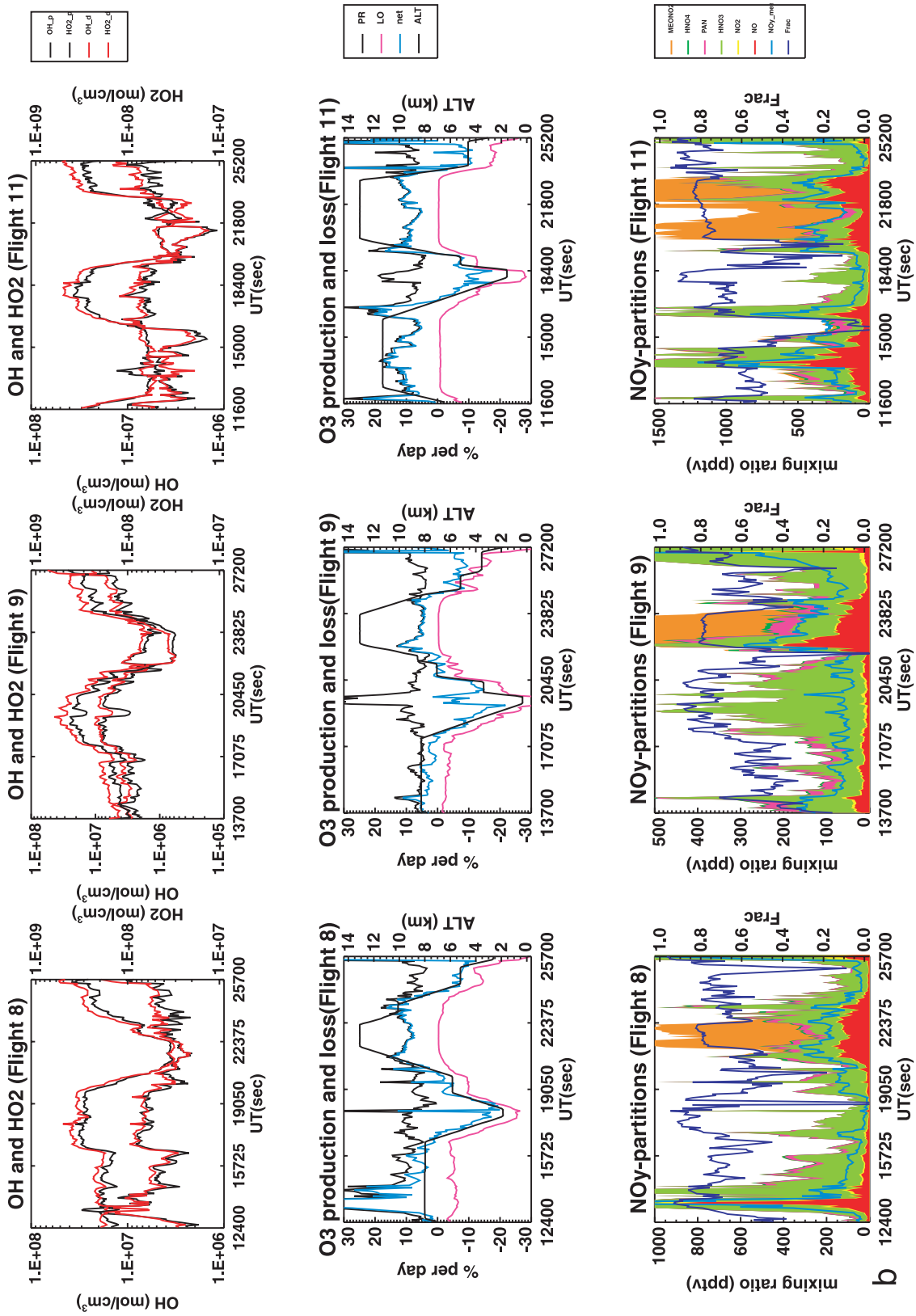

Figure 3. (continued)

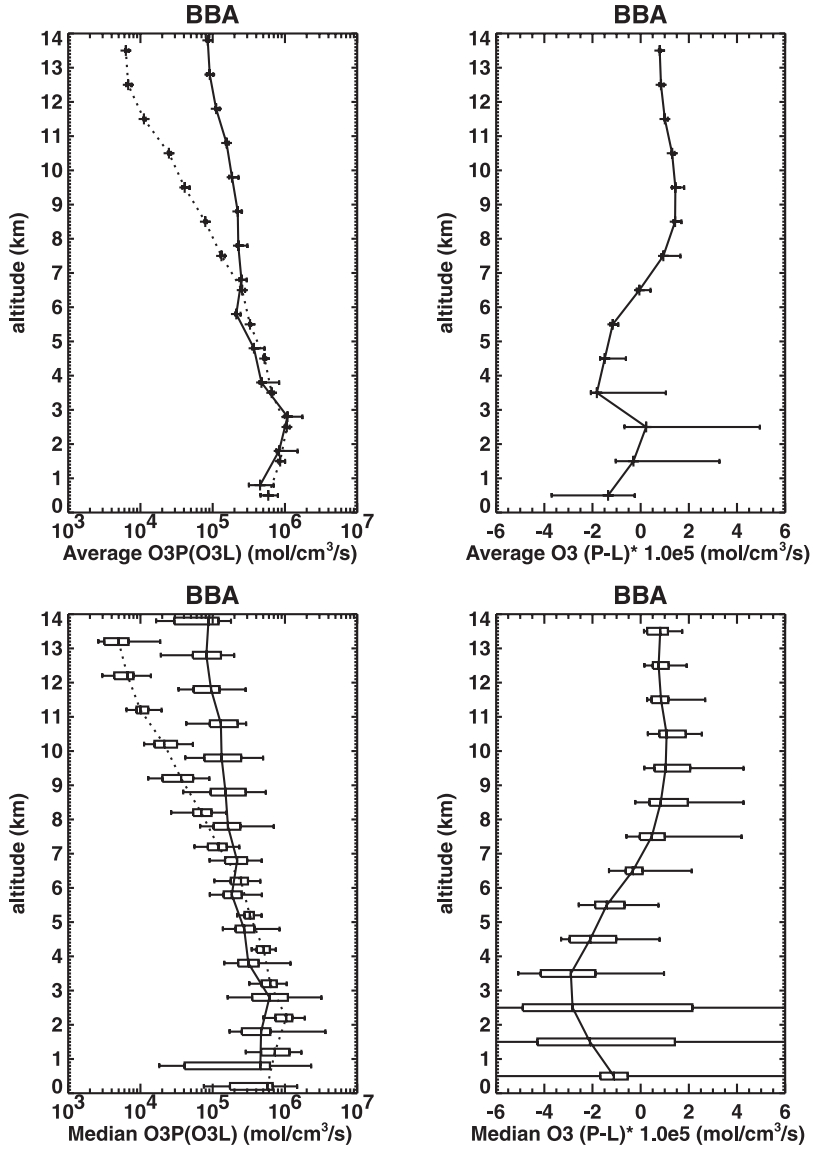

Figure 4. Mean and median values for ozone production, removal, and net production rates as functions of altitude for BIBLE A. The bar on the mean profile represents the standard deviation, calculated separately for points larger and smaller than the averaged values. The box on the median profile represents points whose values are 25% larger and smaller than the median. The whisker gives the 5% to 95% of the data. Values plotted are average (mean) values for each altitude bin. The two curves in each of the left panels are production (solid) and removal rate (dotted). Note that the points are plotted at slightly different altitudes for clarity.

factor of 2 of the true value while the uncertainty for $\langle L \rangle$ should be smaller.

5. Comparison of Model Calculated NO_y and Observed NO_y

[27] We define equilibrium concentration of NOy ($[NOy]_{equil}$) to be

$$[NOy]_{equil} = n^{II}_{NO}(t_{obs}) + n^{II}_{HNO_3}(t_{obs}) + n^{II}_{PAN}(t_{obs}) + n^{II}_{NO_2}(t_{obs}) + n^{II}_{HNO_4}(t_{obs}) + n^{II}_{CH_3O_2NO_2}(t_{obs}) + 2n^{II}_{N_2O_5}(t_{obs}) + n^{II}_{NO_3}(t_{obs})$$

where the $n^{II}_j(t)$ are obtained as defined in section 4.1. Note that $[NOy]_{equil}$ is constant in time and can be defined using $n^{II}_j(t)$ at any time of the day. The third row in Figure 3 shows the measured NO concentration ($[NO]_{meas}$), $n^{t_{obs}}_{NO_2} = n^{II}_{NO}(t_{obs}) + n^{II}_{NO_2}(t_{obs}) - [NO]_{meas}$, along with the model calculated concentrations of the other NO_y species: HNO_3, PAN, HNO_4, and $CH_3O_2NO_2$ from $n^{II}_j(t_{obs})$ along the flight track. Concentrations for N_2O_5 and NO_3 are too small to show. The measured concentration of NO_y ($[NO_y]_{meas}$) is also plotted in Figure 3 represented by the thick blue line. Note that $[NO_y]_{meas}$ and $[NO_y]_{equil}$ are in reasonably good agreement (within a factor of 2) except above 12 km and below 2 km. At high altitudes, $[NO_y]_{equil}$ is dominated by $n_{CH_3O_2NO_2^{II}}(t_{obs})$. Near the ground $n^{II}_{HNO_3}(t_{obs})$, dominates. The high concentrations above 12 km calculated for $CH_3O_2NO_2$ result from the adopted reaction rate constants.

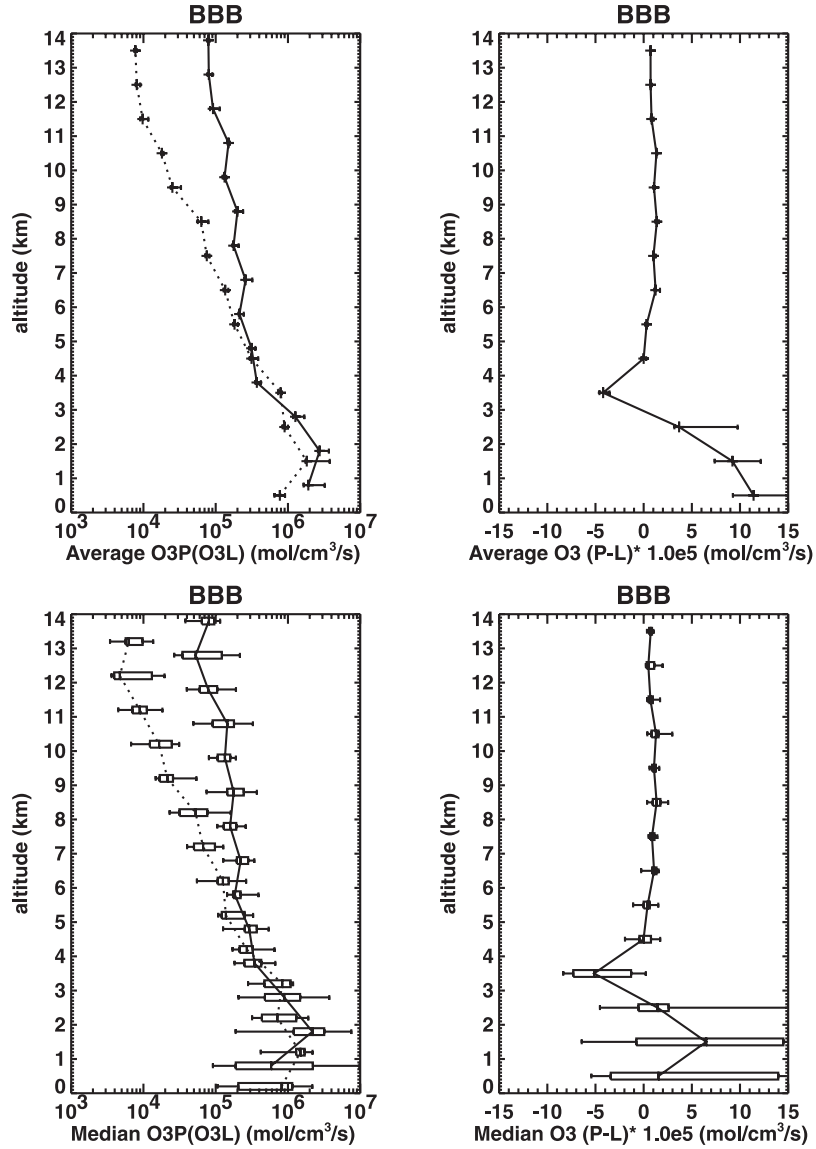

Figure 5. Same as Figure 4 but for BIBLE B.

With recommended temperature dependence of the equilibrium constant for $CH_3O_2NO_2$, the decomposition rate at 12 km is a factor of 10 smaller than the rate at 11 km. We varied the rate within the uncertainty limit cited in JPL-97 to determine how $[CH_3O_2NO_2]$ may change. The calculated concentration of $CH_3O_2NO_2$ becomes negligible when the faster rate is adopted. The difference at low altitudes is most likely due to the fact that our method does not account for scavenging of HNO_3.

[28] If we ignore the results for 12 km, HNO_3 is the dominant contributor to $[NO_y]_{equil}$ with *PAN* playing a substantial role in certain situations. Also plotted with the bottom panel in Figure 3 is the parameter $Frac = 1 - \frac{[NO_y]_{meas}}{[NO_y]_{equil}}$. Given $[NO_y]_{meas}$ at a sampling point, one can use $\{n_j^{II}(t)\}$ from the diurnal model to compute

$$n_{NO_X}^{eq}(t_{obs}) = [NO_y]_{meas} \times \frac{n_{NO}^{II}(t_{obs}) + n_{NO_2}^{II}(t_{obs})}{[NO_y]_{equil}}, \qquad (6)$$

where $n_{NO_X}^{eq}(t_{obs})$ is the NOx concentration that is in equilibrium with $[NO_y]_{meas}$. The quantity $\Delta[NO_X] = [NO]_{meas} + n_{NO_2}^{t_{obs}} - n_{NO_X}^{eq}(t_{obs})$ is related to *Frac* via

$$\frac{\Delta[NO_x]}{[NO]_{meas}+n_{NO_2}^{t_{obs}}} = 1 - \frac{n_{NO_X}^{eq}(t_{obs})}{[NO]_{meas}+n_{NO_2}^{t_{obs}}} = 1 - \frac{[NO_y]_{meas}}{[NO_y]_{equil}} = Frac$$

where we used equation (6) and the relationship $[NO]_{meas} + n_{NO_2}^{t_{obs}} = n_{NO}^{II}(t_{obs}) + n_{NO_2}^{II}(t_{obs})$ in the last step. A nonzero value for $\Delta[NO_x]$ would signal that the air parcel is not in photochemical equilibrium. This could occur for a number of reasons. First, it could be due to recent injection of NO into the parcel. Alternatively, this could be a result of the recent scavenging of NOy rather than injection of NO. This most likely has the largest impact below 5 km. Finally, a sampled parcel could have been recently transported from another location and thus is still adjusting to the new photochemical environment.

Table 1. Column-Integrated Mean and Median Production, Removal and Net Rates for Ozone[a]

Data Sorted by Latitudes	Number of Data Points	Production, 10^{11} molecules/cm^2/s	Removal, 10^{11} molecules/cm^2/s)	Net, 10^{11} molecules/cm^2/s
		BIBLE A		
All	2200	4.2/2.8	3.9/3.7	0.27/−0.64
Ferry (north of equator)	390	2.0/1.7	2.9/2.9	−0.9/−0.98
Indonesian (equator to 10°S)	1200	4.8/3.2	3.9/3.6	0.92/−0.44
Australia (south of 10°S)	580	4.3/3.2	4.5/4.1	−0.18/−0.98
		BIBLE B		
All	1530	6.3/5.1	4.6/4.0	1.2/1.1
Ferry (north of equator)	415	4.0/3.5	2.6/2.5	1.5/0.45
Indonesian (equator to 10°S)	225	2.9/2.4	2.4/2.4	0.50/−0.13
Australia (south of 10°S)	890	6.6/5.5	4.7/4.2	1.9/1.2

[a]Values are obtained by integrating the mean values for each altitude from 1 km to 14 km. Data between 0 km and 1 km are not included. The table entry corresponds to mean/median.

[29] Given the accuracy of the measurements, we estimate that it is only possible to confidently distinguish the derived value of $\Delta[NO_x]$ from zero for those sampling points where $\frac{[NO_y]_{equil}}{[NO_y]_{meas}} > 1.2$ or $Frac > 0.17$. Using this criteria, less than 10% of the sampled points are in equilibrium. Above 10 km, 50% of the sampled points have $\frac{[NO_y]_{equil}}{[NO_y]_{meas}} > 1.7$ or $Frac > 0.4$. Given the assumption we used to calculate $[NO_y]_{equil}$, it seems more reasonable to use this latter criterion to identify recently perturbed air.

[30] We next discuss how the model calculated production rate for ozone $\langle P \rangle$ can be used as another indicator for recent injection of ozone precursors. The values for $\langle P \rangle$ along the flight track are plotted in the second row in Figure 3. The results are plotted in units of percent per day, which is more directly related to the photochemical age of the air parcel as ozone adjusts to injected precursors. Equation (1) shows that an air parcel with recent injection of NO and RO_2 would have a high value for ozone production.

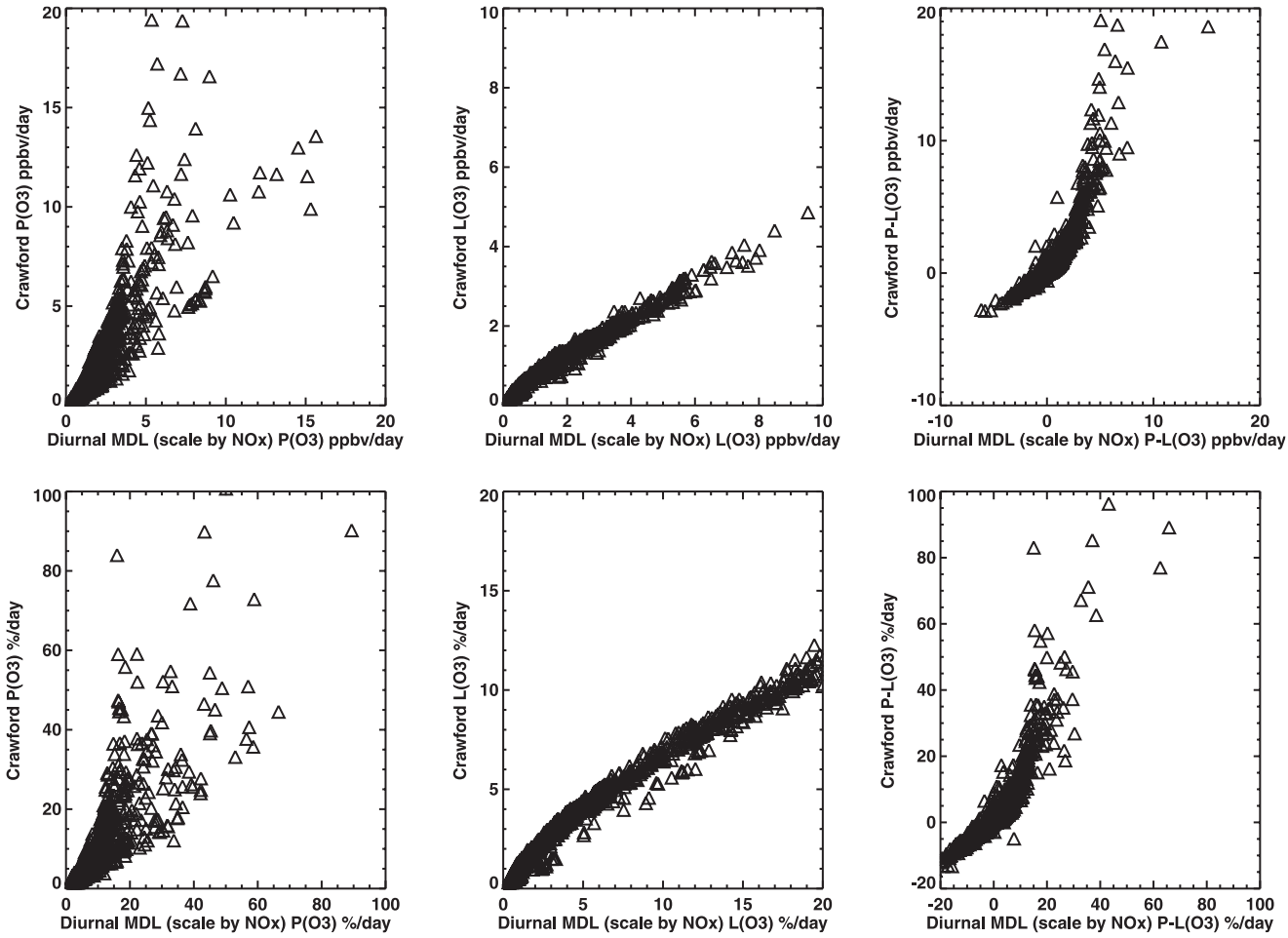

Figure 6. Comparison of the diurnal averaged production ($\langle P \rangle$), removal ($\langle L \rangle$) and net ($\langle P \rangle$-$\langle L \rangle$) rates of ozone with values obtained using the *Crawford et al.* [1997b] parameterization. Values are calculated using BIBLE B data.

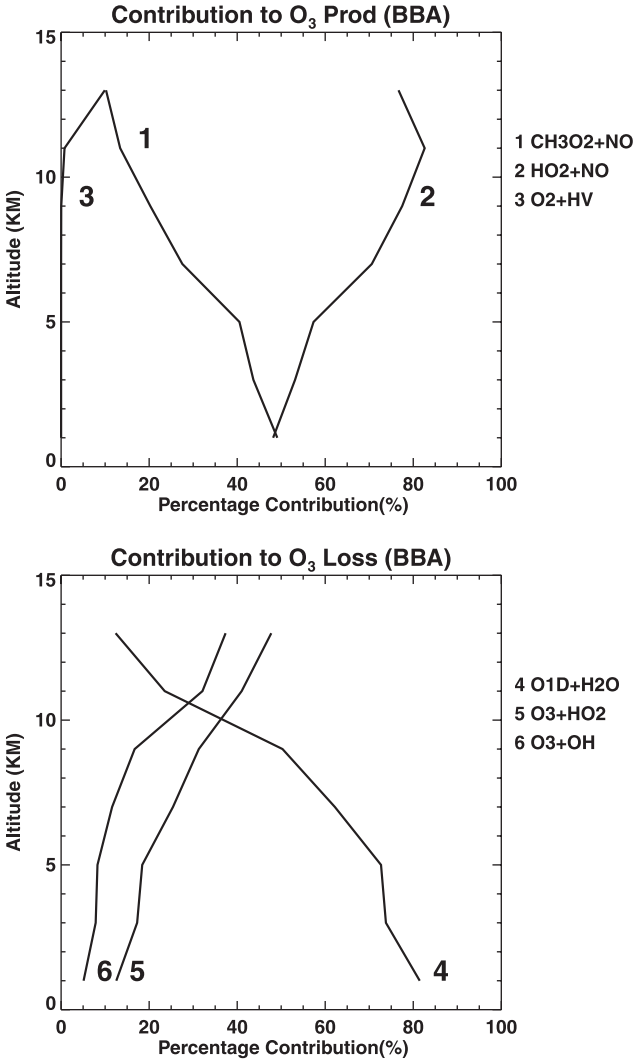

Figure 7. Model calculated percent contributions to the diurnal averaged production and removal rates of ozone as functions of altitude for BIBLE A. The values shown correspond to the mean values for each 2 km altitude bin.

The production value will remain high until NO_x is converted to HNO_3 and the RO_2 are removed by some chain termination step. In the mean time, ozone concentration will be increasing. This argument suggests that, immediately after the injection, the production rate is high while the ozone concentration is still low. Thus $\langle P \rangle$ in %/day, which corresponds to the net production rate divided by the ozone concentration, should be a better indicator of recent NO injection.

[31] Figure 9 shows an example of the scatterplot of the ratio of $\frac{[NO_y]_{equil.}}{[NO_y]_{meas}}$ versus $\langle P \rangle$ for sampling points between 8 and 9 km from BIBLE A. There were 394 points from the 1-min file that satisfy the criteria having SZA less than 60°. Twenty-four of the points have $\langle P \rangle$ values larger than 20%/day and are not displayed in the Figure 9. Only 5% of the points shown in Figure 9 have $\frac{[NO_y]_{equil}}{[NO_y]_{meas}} < 1.2$. Figures 9b and 9c show the probability distribution functions of the sampled points in $\langle P \rangle$ and in $\frac{[NO_y]_{equil}}{[NO_y]_{meas}}$, respectively. Based on these results and the fact that the production rate for ozone in an aged parcel is of order 5%/day, we will argue that only points with $\frac{[NO_y]_{equil}}{[NO_y]_{meas}} > 2$ and $\langle P \rangle$ >5%/day are likely to have experienced recent NO injection. Points from flights over the oceans (flights 3, 14 and 15) and flights over Australia (flights 4–6) have small values of $\langle P \rangle$. Flights out of Bandung over land area have large values of $\langle P \rangle$ and are mostly indicative of air mass still adjusting to recent injection of NO.

6. Future Directions

[32] In this paper, we presented a method for calculating the diurnal averaged production and removal rates of ozone along the flight track. We suggested that the production rate may be a useful indicator of the time elapsed since the last injection of NO. We have yet to make use of the available information on back-trajectories of air parcels. It is possible to estimate the source terms for NO_x from lightning and biomass burning [see, e.g., *Koike et al.*, 2002] and use the photochemical air trajectory model to compute the expected concentrations of the trace species at the sampling point [see, e.g., *Kita et al.*, 2002]. Comparison of the calculated

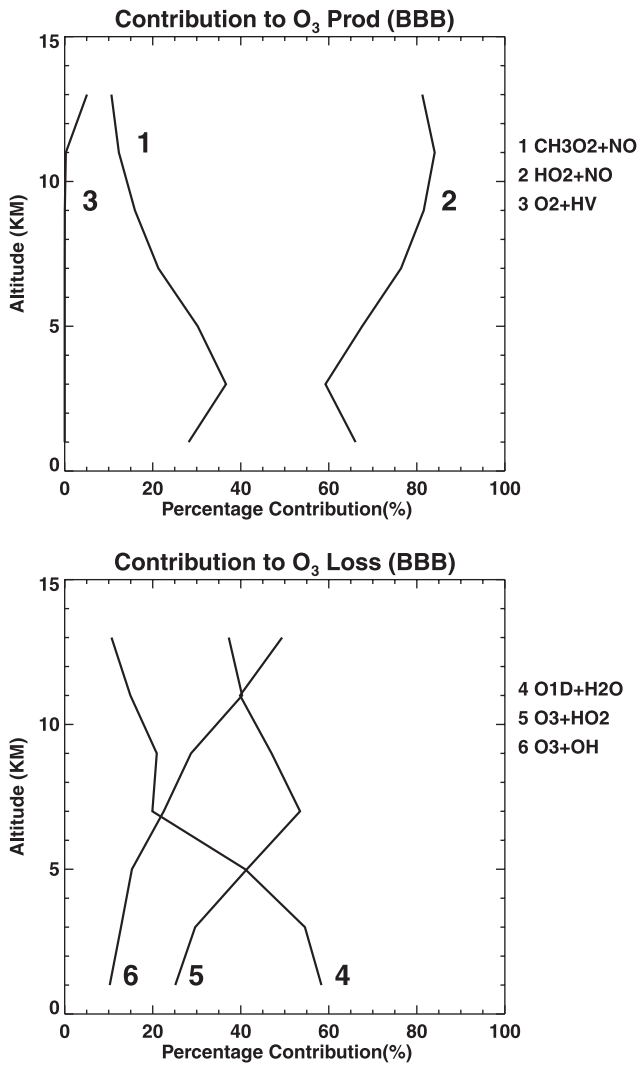

Figure 8. Same as Figure 7 except for BIBLE B.

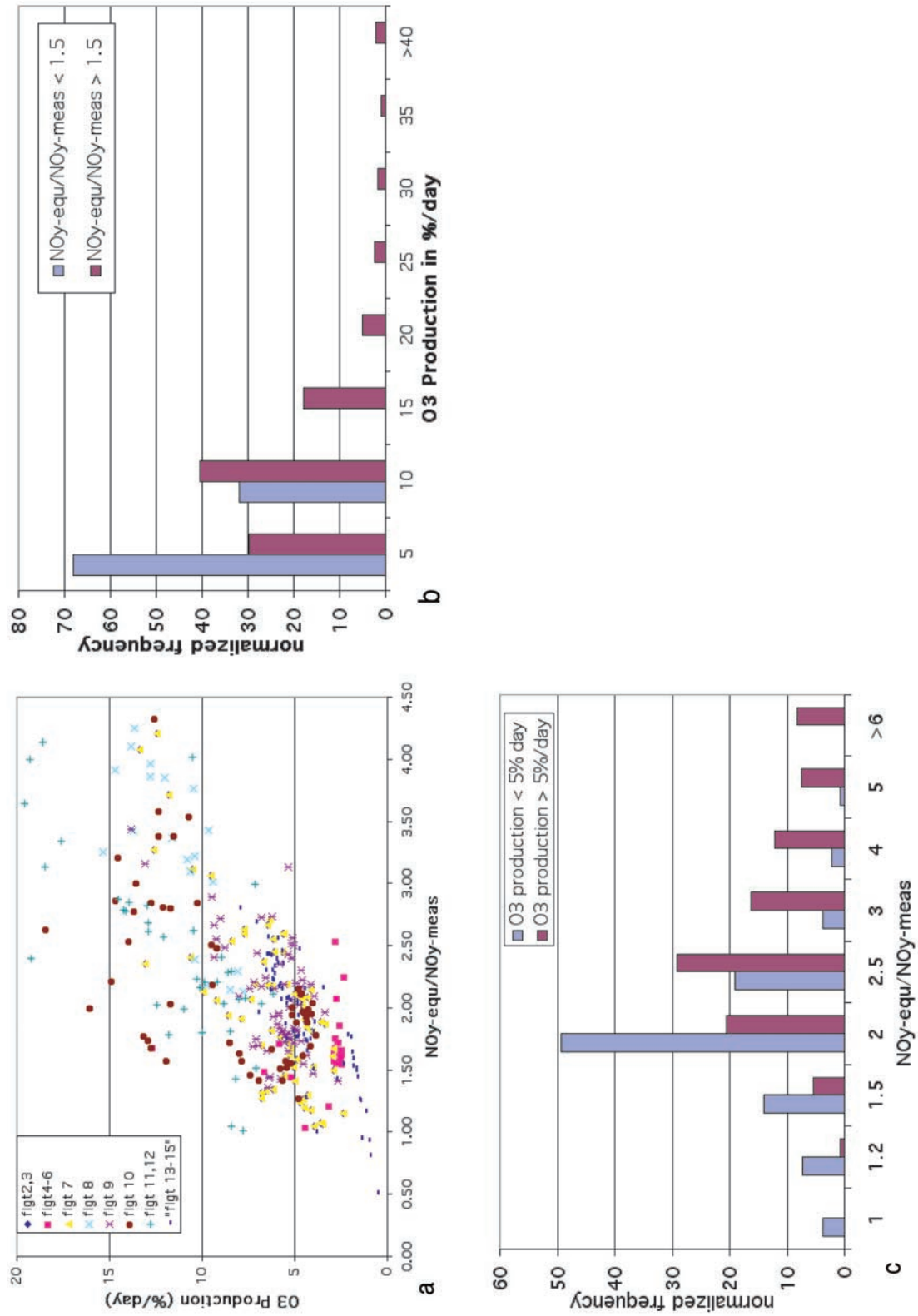

Figure 9. (a) Scatterplot of the ratio $\frac{[NO_y]_{equ}}{[NO_y]_{meas}}$ versus ozone production rates between 8 and 9 km for all BIBLE A data. (b) Frequency of occurrence for ozone production rate in percent per day. (c) Frequency of occurrence for $\frac{[NO_y]_{equ}}{[NO_y]_{meas}}$. (b) Normalized frequency of occurrence in ozone production rate (%/day) for two groups of data segregated according to whether $\frac{[NO_y]_{equ}}{[NO_y]_{meas}}$ is larger or smaller than 1.5. The frequency of occurrence is normalized to 100 for each group. (c) Normalized frequency of occurrence in $\frac{[NO_y]_{equ}}{[NO_y]_{meas}}$ for two groups of data segregated according to whether the ozone production rate is larger or smaller than 5%/day. The frequency of occurrence is normalized to 100 for each group.

values with the measured values should provide information on the origin of the air parcel and help validate the estimated source strengths used in the calculation. Such analyses will better constrain the (unmeasured) concentrations used to initialize the air trajectory calculations. With the constrained initial conditions, the photochemical air trajectory model can then be used to compute the average net production for ozone for the parcel history.

[33] **Acknowledgments.** Work supported by the Earth Observation Research Center of the National Space Development Agency of Japan. Analysis of the data at AER is also supported by the Atmospheric Chemistry Modeling and Analysis Program (NAS1-00138) of the National Aeronautics and Space Administration of the U.S. We would like to thank the reviewers for making many constructive suggestions that greatly improved the paper.

References

Brune, W. H., et al., Airborne in situ OH and HO_2 observations in the cloud-free troposphere and lower stratosphere during SUCCESS, *Geophys. Res. Lett.*, *25*, 1701–1704, 1998.

Brune, W. H., et al., OH and HO_2 chemistry in the North Atlantic free troposphere, *Geophys. Res. Lett.*, *26*, 3077–3080, 1999.

Crawford, J., et al., Implications of large scale shifts in tropospheric NO_x levels in the remote tropical Pacific, *J. Geophys. Res.*, *102*, 28,447–28,468, 1997a.

Crawford, J., et al., An assessment of ozone photochemistry in the extratropical western North Pacific: Impact of continental outflow during the late winter/early spring, *J. Geophys. Res.*, *102*, 28,469–28,487, 1997b.

Crawford, J., et al., Assessment of upper tropospheric HO_x sources over the tropical Pacific based on NASA GTE/PEM data: Net effect on HO_x and other photochemical parameters, *J. Geophys. Res.*, *104*, 16,255–16,274, 1999.

Davis, D. D., et al., Assessment of ozone photochemistry in the western North Pacific as inferred from PEM-West A observations during the fall 1991, *J. Geophys. Res*, *101*, 2111–2134, 1996.

DeMore, W. B., S. P. Sander, D. M. Golden, R. F. Hampson, M. J. Kurylo, C. J. Howard, A. R. Ravishankara, C. E. Kolb, and M. J. Molina, Chemical kinetics and photochemical data for use in stratospheric modeling: Evaluation number 12, *JPL Publ., 97-4*, 1997.

Fahey, D. W., et al., Ozone destruction and production rates between spring and autumn in the Arctic stratosphere, *Geophys. Res. Lett.*, *27*, 2605–2608, 2000.

Folkins, I., et al., OH and HO_2 in two biomass burning plumes: sources of HO_x and implications for ozone production, *Geophys. Res. Lett.*, *24*, 3185–3188, 1997.

Galanter, M., H. Levy II, and G. R. Carmichael, Impacts of biomass burning on tropospheric CO, NO_x, and O3, *J. Geophys. Res.*, *105*, 6633–6653, 2000.

Jaegle, L., et al., Sources of HO_x and production of ozone in the upper troposphere over the United States, *Geophys. Res. Lett.*, *25*, 1709–1712, 1998.

Jaegle, L., D. J. Jacob, W. H. Brune, and P. O. Wennberg, Chemistry of HO_x radicals in the upper troposphere, *Atmos. Environ.*, *35*, 469–489, 2001.

Jacob, D. J., et al., Origin of ozone and NO_x in the tropical troposphere: A photochemical analysis of aircraft observations over the South Atlantic Basin, *J. Geophys. Res.*, *101*, 24,235–24,250, 1996.

Kiem, E. R., et al., NO_y partitioning from measurements of nitrogen and hydrogen radicals in the upper troposphere, *Geophys. Res. Lett.*, *26*, 51–54, 1999.

Kita, K., et al., Photochemical production of ozone in the upper troposphere in association with cumulus convection over Indonesia, *J. Geophys. Res.*, doi:10.1029/2001JD000844, in press, 2002.

Klonecki, A. A., and H. Levy II, Tropospheric chemical ozone tendencies in $CO\text{-}CH_4\text{-}NO_y\text{-}H_2O$ system: Their sensitivity to variations in environmental parameters and their application to a global chemistry transport model study, *J. Geophys. Res.*, *102*, 21,221–21,237, 1997.

Koike, M., et al., Reactive nitrogen over the tropical western Pacific: Influence from lightning and biomass burning during BIBLE A, *J. Geophys. Res.*, doi:10.1029/2001JD000823, in press, 2002.

Kondo, Y., M. Ko, M. Koike, S. Kawakami, and T. Ogawa, Preface, *J. Geophys. Res.*, doi:10.1029/2002JD002401, in press, 2002a.

Kondo, Y., et al., Effects of biomass burning, lightning, and convection on O_3, CO, and NO_y over the tropical Pacific and Australia in August–October 1998 and 1999, *J. Geophys. Res.*, doi:10.1029/2001JD000820, in press, 2002.

Kotamarthi, V. R., et al., Evidence of heterogeneous chemistry on sulfate aerosols in stratospherically influenced air masses sampled during PEM West-B, *J. Geophys. Res.*, *102*, 28,425–28,436, 1997.

Levy, H., II, W. J. Moxim, A. A. Klonecki, and P. S. Kasibhatla, Simulated tropospheric NO_x: Its evaluation, global distribution and individual source contributions, *J. Geophys. Res.*, *104*, 26,279–26,306, 1999.

Liu, S. C., et al., Sources of reactive nitrogen in the upper troposphere during SONEX, *Geophys. Res. Lett.*, *26*, 2441–2444, 1999.

McKeen, S. A., E.-Y. Hsie, M. Trainer, R. Tallamraju, and S. C. Liu, A regional model study of the ozone budget in the eastern United States, *J. Geophys. Res.*, *96*, 10,809–10,845, 1991.

McKeen, S. A., et al., The photochemistry of acetone in the upper troposphere: A source of odd-hydrogen radicals, *Geophys. Res. Lett.*, *24*, 3177–3180, 1997.

Price, C., J. Penner, and M. Prather, NO_x from lightning, 1, Global distribution based on lightning Physics, *J. Geophys. Res.*, *102*, 5929–5942, 1997.

Schultz, M. G., et al., On the origin of tropospheric ozone and NO_x over the tropical Pacific, *J. Geophys. Res.*, *104*, 5829–5843, 1999.

Singh, H. B., et al., High concentrations and photochemical fate of oxygenated hydrocarbons in the global troposphere, *Nature*, *368*, 50–54, 1995.

Takegawa, N., et al., Correlation of trace gases in biomass burning, plumes in the boundary layer over Northern Australia, *J. Geophys. Res.*, doi:10.1029/2002JD002505, in press, 2002.

Wennberg, P. O., et al., Removal of stratospheric O_3 by radicals: In situ measurements of OH, HO_2, NO, NO_2, ClO and BrO, *Science*, *266*, 398–404, 1994.

D. R. Blake, Department of Chemistry, University of California, Irvine, CA 92697-2025, USA. (dblake@orion.oac.uci.edu)

W. Hu, Virginia Department of Environmental Quality, Richmond, VA 23240, USA. (whu@deq.state.va.us)

S. Kawakami and T. Ogawa, Earth Observation Research Center, National Space Development Agency of Japan, 1-8-10 Harumi, Chuouku, Tokyo 106-0032, Japan. (kawakami@eorc.nasda.go.jp; t_ogawa@eorc.nasda.go.jp)

K. Kita and Y. Kondo, Research Center for Advanced Science and Technology, University of Tokyo, 4-6-1 Komaba, Meguro-ku, Tokyo 153-8904, Japan. (kita@sunepl.geoph.s.u-tokyo.ac.jp; kondo@atmos.rcast.u-tokyo.ac.jp)

M. Ko, NASA Langley Research Center, MS 401B, Hampton, VA 23681-2199, USA. (m.k.ko@larc.nasa.gov)

M. Koike, Department of Earth and Planetary Science, Graduate School of Science, University of Tokyo, 7-3-1 Hongo, Bunkyo-ku, Tokyo 113-0033, Japan. (koike@eps.s.u-tokyo.ac.jp)

S. Liu, Institute of Earth Sciences, Academia Sinica, Taipei 110, Taiwan. (shawliu@earth.sinica.edu.tw)

J. M. Rodríguez, Rosenstiel School of Marine and Atmospheric Science, University of Miami, Miami, FL 33149, USA. (jrodriguez@rsmas.miami.edu)